Total-Body PET and Highly Stable Chelators Together Enable Meaningful [89]Zr-Antibody PET Studies up to 30 Days After Injection

Eric Berg[1], Herman Gill[2], Jan Marik[2], Annie Ogasawara[2], Simon Williams[2], Guus van Dongen[3], Daniëlle Vugts[3], Simon R. Cherry[1,4], and Alice F. Tarantal[5]

[1]Department of Biomedical Engineering, University of California–Davis, Davis, California; [2]Department of Biomedical Imaging, Genentech Inc., South San Francisco, California; [3]Department of Radiology and Nuclear Medicine, Amsterdam UMC, VU University, Amsterdam, The Netherlands; [4]Department of Radiology, School of Medicine, University of California–Davis, Davis, California; and [5]Department of Pediatrics and Department of Cell Biology and Human Anatomy, School of Medicine, and California National Primate Research Center, University of California–Davis, Davis, California

See an invited perspective on this article on page 451.

The use of [89]Zr-antibody PET imaging to measure antibody biodistribution and tissue pharmacokinetics is well established, but current PET systems lack the sensitivity needed to study [89]Zr-labeled antibodies beyond 2–3 isotope half-lives (7–10 d), after which a poor signal-to-noise ratio is problematic. However, studies across many weeks are desirable to better match antibody circulation half-life in human and nonhuman primates. These studies investigated the technical feasibility of using the primate mini-EXPLORER PET scanner, making use of its high sensitivity and 45-cm axial field of view, for total-body imaging of [89]Zr-labeled antibodies in rhesus monkeys up to 30 d after injection. **Methods:** A humanized monoclonal IgG antibody against the herpes simplex viral protein glycoprotein D (gD) was radiolabeled with [89]Zr via 1 of 4 chelator-linker combinations (benzyl isothiocyanate-DFO [DFO-Bz-NCS], where DFO is desferrioxamine B; DFO-squaramide; DFO*-Bz-NCS, where DFO* is desferrioxamine*; and DFO*-squaramide). The pharmacokinetics associated with these 4 chelator-linker combinations were compared in 12 healthy young male rhesus monkeys (~1–2 y old, ~3 ± 1 kg). Each animal was initially injected intravenously with unlabeled antibody in a peripheral vessel in the right arm (10 mg/kg, providing therapeutic-level antibody concentrations), immediately followed by approximately 40 MBq of one of the [89]Zr-labeled antibodies injected intravenously in a peripheral vessel in the left arm. All animals were imaged 6 times over a period of 30 d, with an initial 60-min dynamic scan on day 0 (day of injection) followed by static scans of 30–45 min on approximately days 3, 7, 14, 21, and 30, with all acquired using a single bed position and images reconstructed using time-of-flight list-mode ordered-subsets expectation maximization. Activity concentrations in various organs were extracted from the PET images using manually defined regions of interest. **Results:** Excellent image quality was obtained, capturing the initial distribution phase in the whole-body scan; later time points showed residual [89]Zr mainly in the liver. Even at 30 d after injection, representing approximately 9 half-lives of [89]Zr and with a total residual activity of only 20–40 kBq in the animal, the image quality was sufficient to readily identify activity in the liver, kidneys, and upper and lower limb joints. Significant differences were noted in late time point liver uptake, bone uptake, and whole-body clearance between chelator-linker types, whereas little variation (±10%) was observed within each type. **Conclusion:** These studies demonstrate the ability to image [89]Zr-radiolabeled antibodies up to 30 d after injection while maintaining satisfactory image quality, as provided by the primate mini-EXPLORER with high sensitivity and long axial field of view. Quantification demonstrated potentially important differences in the behavior of the 4 chelators. This finding supports further investigation.

Key Words: PET; immuno-PET; quantification; total-body imaging; rhesus monkey

Extending human and nonhuman primate PET studies beyond 7–10 d after injection at an acceptable radiation exposure is currently impractical even with a positron-emitting isotope that has an appropriately long half-life, such as [89]Zr. [89]Zr is the positron emitter of choice for PET imaging of slow-kinetic drugs such as monoclonal antibodies, and for this purpose [89]Zr has to be stably coupled to the antibody via a chelate. Beyond 2–3 physical half-lives, however, most contemporary commercial scanners are not sufficiently sensitive to collect the necessary coincidence events from the residual [89]Zr in the subject to reconstruct images with a signal-to-noise ratio high enough to allow accurate image interpretation and quantification. Although longer scans can compensate for decay by collecting more coincidence events, this option quickly becomes prohibitive in studies that require sedation or when the scan duration is limited by patient comfort, motion, and clinical demands. Therefore, the physical ability to acquire images at later time points depends primarily on the development of PET scanners with significantly higher sensitivity than those currently available. Once they are developed, executing biologically meaningful late-time point studies will depend on the availability of radiotracer molecules such as [89]Zr-chelates that maintain their integrity in the body over the multiweek time scale of the study. The investigations described herein illustrate the successful combination of a new total-body PET scanner and novel chelator moieties for [89]Zr.

There have been several recent developments in high-sensitivity PET systems that are suitable for human and nonhuman primate imaging (1–4). In these scanners, substantial sensitivity gains have been achieved by extending the scanner's axial length up to approximately 2 m for a human imaging system and to approximately 50 cm in preclinical systems. In this study, we have used the primate mini-EXPLORER PET system, a 45-cm-long system with National Electrical Manufacturers Association NU-2 sensitivity of approximately 50 kcps/MBq, which is capable of imaging the entire body of young rhesus monkeys in a single bed position (1,5).

PET provides a unique methodology to quantitatively image the biodistribution and kinetics associated with a wide range of molecules in vivo, from metabolites to nanoparticles. An increasingly common application is the imaging of radiolabeled antibodies ("antibody PET"), now an established technique to gain understanding of the behavior of antibodies and their target antigens noninvasively and to inform, for example, early readouts of the efficacy of novel antibody-based immunotherapies (6–8). Since the terminal half-life of therapeutic antibodies in humans is commonly on the order of one to several weeks, the desired imaging time points can extend over the same time scale to fully determine the fate of the tracer antibodies. In addition to antibodies, other emerging applications that rely on late-time-point PET acquisition include imaging the biodistribution of transplanted stem and/or progenitor cells, chimeric antigen receptor T cells (9,10), and radiolabeled nanoparticles (11,12). For stem cell and progenitor cell applications, imaging time points can be up to 2–5 wk after injection in order to efficiently capture the early biodistribution of the cells that is critically important in evaluating cell trafficking, engraftment, safety, and outcomes over time.

Extending the duration of PET studies beyond 7–10 d after the delivery of a radiolabeled imaging agent does present some challenges. The first is the need for a positron-emitting isotope with a sufficiently long radioactive half-life that is well matched to the biologic half-life and uptake time of the imaging agent. Several radioisotopes have been investigated for long-duration PET studies, including ^{64}Cu and ^{124}I, although ^{89}Zr best fulfills many of the desired properties with its 3.27-d half-life. In addition, other favorable physical properties include minimal contamination from the 909-keV prompt γ-photons within the 511-keV PET energy window, as well as superior spatial resolution compared with many other positron-emitting isotopes as a result of the relatively low excess decay energy (mean energy, 396 keV). Chemically, the facile incorporation of ^{89}Zr by chelation and the residualizing behavior of ^{89}Zr are often preferred to the covalent labeling reactions and nonresidualizing behavior of ^{124}I. As such, ^{89}Zr is now often used to characterize the in vivo behavior of slow-kinetic molecules by PET, including antibodies and single-domain antibodies (13–15).

A challenge associated with ^{89}Zr in studies at late time points lies in minimizing the release of osteophilic ^{89}Zr ions or low-molecular-weight catabolites from the imaging agent (i.e., antibody, cell, nanoparticle). Progressively liberated ^{89}Zr catabolites, potentially free ^{89}Zr^{4+}, have often been observed to accumulate irreversibly in mineralized bone, especially at sites of active bone remodeling such as the joints, which can complicate image interpretation (16). These observations are most dominant in preclinical PET studies, with less bone signal observed in clinical studies in general.

Several chelators have been investigated for use in ^{89}Zr-PET studies (17), but desferrioxamine B (DFO) remains the most widely adopted. DFO is available commercially with either of 2 lysine-reactive bifunctional linkers, benzyl isothiocyanate-DFO (DFO-Bz-NCS) or

tetrafluorophenyl-N-succinyl-DFO (18,19), and has been applied in a variety of ^{89}Zr-PET applications, including human clinical studies (20,21). However, in vivo PET imaging studies with ^{89}Zr-DFO suggest less than ideal stability beyond approximately 3 d (14). This lack of stability is a consequence of the hexadentate binding complex provided by DFO—a type of binding that is not ideally matched to ^{89}Zr^{4+}, which prefers formation of octadentate binding, which occupies all available coordination sites of ^{89}Zr^{4+}. An octadentate variant of DFO, desferrioxamine* (DFO*), was recently developed through the addition of a fourth hydroxamate unit to the chelator (22,23). In vivo studies with mice and ^{89}Zr-DFO*-antibodies have demonstrated reduced ^{89}Zr signal in the bone and liver. A potential alternative route to achieve octadentate binding of ^{89}Zr^{4+} is through the linker. A new linker, using a squaramide moiety (24), was recently developed on the premise of using a linker that contributes oxygen molecules to the DFO chelator to achieve octadentate ^{89}Zr binding. Indeed, DFO-squaramide showed promising in vivo results in ^{89}Zr-PET studies with mice. However, a robust comparison of the in vivo pharmacokinetics associated with the ^{89}Zr chelator-linker combinations most often used clinically is lacking and therefore represents a critically needed step toward enabling long-duration ^{89}Zr-PET studies.

The aim of this study was twofold. The primary goal was to demonstrate the feasibility of extending nonhuman primate ^{89}Zr PET studies to 30 d after injection by using the high-sensitivity primate mini-EXPLORER total-body PET system. In addition, we used the late-time-point imaging capabilities of EXPLORER to quantify the pharmacokinetics associated with 4 ^{89}Zr chelator-linker combinations based on DFO or DFO* chelators and Bz-NCS or squaramide linkers. We initiated these studies to begin examining their suitability for long-duration PET studies by assessing pharmacokinetics and the image signal at the joints as an indicator of osteophilic catabolite formation.

MATERIALS AND METHODS

Chelator-Linkers, Antibodies, and Radiolabeling

Four ^{89}Zr chelator-linker moieties were compared: DFO-Bz-NCS, DFO*-Bz-NCS, DFO-squaramide, and DFO*-squaramide (chemical structures are provided in Supplemental Fig. 1; supplemental materials are available at http://jnm.snmjournals.org). Common solvents and chemicals were purchased from Aldrich or VWR International, if not stated otherwise. DFO-Bz-NCS was purchased from Macrocyclics. DFO-squaramide was prepared according to the procedure published in Rudd et al. (24). DFO* was prepared by the procedure described by Patra et al. (23). DFO*-Bz-NCS was synthesized as described by Vugts et al. (22). Anti-gD antibody (specific to glycoprotein D on the herpes simplex virus) was prepared at Genentech, Inc. ^{1}H nuclear magnetic resonance spectra were acquired on a Bruker Avance II 400 spectrometer at 298 K, and the chemical shifts are reported in parts per million relative to tetramethylsilane.

The following systems were used to analyze and purify the products. System A (analytic liquid chromatography–mass spectrometry) used a Waters Acquity ultra-performance liquid chromatography running at 0.7 mL/min. The column was an Acquity ultra-performance liquid chromatography BEH C18 (1.7 μm, 2.1 × 30 mm). Mobile phase A was water with 0.1% formic acid, and B was acetonitrile with 0.1% formic acid; the linear gradient was 5%–95% B in 2 min. The system was equipped with an Acquity photodiode array and Acquity single-quadrupole detectors. System B (preparative high-performance liquid chromatography) used an Interchim PuriFlash pump running at 60 mL/min. The column was a Phenomenex Gemini-NX (10 μm, C18, 110Å, 100 × 30.00 mm). Mobile phase A was water with 0.1% formic acid, and B was

acetonitrile. The linear gradient was 5%–50% B in 10 min. System C (size-exclusion high-performance liquid chromatography) used an Agilent ultra-performance liquid chromatography system with an in-line diode array detector and radiation detector (Eckert and Ziegler). The column was a TSKgel UP-SW3000 (4.6 × 300 mm; Tosoh Bioscience). The mobile phase was 150 mM sodium phosphate, 250 mM sodium chloride, and 12% isopropanol, pH 7.0. The flow rate was 0.26 mL/min.

DFO*-squaramide was synthesized using the following methodology. DFO* hydrochloride (40 mg, 0.05 mmol) and N,N-diisopropylethylamine (9 μL, 0.05 mmol) were mixed in ethanol (3 mL) and heated to 50°C for 30 min. A solution of diethylsquaramide (25 μL, 0.150 mmol) in ethanol (1.5 mL) was added, and pH was adjusted to 8 by N,N-diisopropylethylamine. The suspension was stirred at 50°C for 3 h. The solvent was removed at reduced pressure, and the residue was dissolved in dimethylsulfoxide (2 mL). The solution was injected onto system B, and collected fractions were evaporated to dryness. Since nuclear magnetic resonance analysis of the product revealed the presence of squaramide, the obtained white solid was washed with acetone to remove the contamination and dried at reduced pressure to provide DFO*-squaramide as a white solid (17 mg, 39%). Liquid chromatography mass spectrometry found the following: m/z 885.4 (calculated for $C_{40}H_{68}N_8O_{14}$, 884.49 Da); purity 96% (ultraviolet, 254 nm); ^{1}H nuclear magnetic resonance (400 MHz, DMSO-d6) δ 9.61 (m, 4H), 8.77 (s, 1H), 8.57 (s, 1H), 7.75 (m, 4H), 4.65 (m, 3H), 3.45 (m, 8H), 3.00 (m, 6H), 2.67 (m, 1H), 2.57 (m, 4H), 2.35–2.30 (m, 1H), 2.27 (m, 6H), 1.96 (s, 3H), 1.57–1.43 (m, 10H), 1.37 (m, 8H), 1.22 (m, 8H).

The conjugation of DFO-Bz-NCS and DFO*-Bz-NCS to anti-gD was performed consistent with Vosjan et al. (25) and Vugts et al. (22). The conjugation of DFO-squaramide and DFO*-squaramide to anti-gD was performed consistent with the method described by Rudd et al. (24). The antibodies were prepared with a conjugate-to-antibody ratio of 1.0–2.0 and a concentration range of 3.7–8.3 mg/mL in succinate formulation buffer (10 mM sodium succinate, 240 mM sucrose, 0.02% polysorbate-20, pH 5.5).

Chelation of ^{89}Zr to each DFO variant was performed consistent with Vosjan et al. (25). The antibodies were prepared at a radioactive concentration range of 47–62 MBq/mL and a protein concentration range of 0.80–1.12 mg/mL in the aforementioned succinate formulation buffer. Specific activities at the end of synthesis ranged from 46 to 77 MBq/mg (DFO-Bz-NCS: 72 MBq/mg; DFO*-Bz-NCS: 58 MBq/mg; DFO-squaramide: 77 MBq/mg; DFO*-squaramide: 46 MBq/mg).

The purity of the ^{89}Zr-labeled DFO variants of anti-gD was measured by system C (Supplemental Fig. 2). Radiolabeling was performed at Genentech South San Francisco, and quality control (QC) measurements were done at several time points up to 7 d after synthesis. However, the ^{89}Zr-antibody samples used for the imaging studies at the University of California–Davis, although from the same batch as the samples used for QC measurements, were stored separately and the QC sample did not undergo transport to the University of California–Davis.

Rhesus Monkey Cohorts

The pharmacokinetics associated with the 4 ^{89}Zr chelator-linker combinations were evaluated in 12 indoor-housed healthy male rhesus monkeys (Table 1). Three animals were used for each chelator-linker type. All animal procedures were performed at the California National Primate Research Center and conformed to the requirements of the Animal Welfare Act, with protocols approved by the Institutional Animal Care and Use Committee at the University of California–Davis.

Imaging Studies

On study day 0 (day of injection) for each chelator-linker type, the animals were injected intravenously with approximately 40 MBq (minimum, 36 MBq; maximum, 47 MBq) of ^{89}Zr-labeled antibody in the left arm (second injection), along with an additional mass dose (10 mg/kg) of unlabeled antibodies injected intravenously in the right arm (first injection). All 3 animals in each group were completed in sequence on the same day. Each animal was placed on the scan bed designed for the primate mini-EXPLORER scanner, carefully positioned, and imaged individually 6 times over 30 d. The imaging time points included the day of injection (day 0) and approximately days 3, 7, 14, 21, and 30 after injection, with scan durations of 60 min for day 0, 45 min for day 30, and 30 min for all intermediate time points. The day 0 PET acquisition was initiated approximately 2 min after injection. A dynamic acquisition using six 10-min frames was included for the day 0 scans.

All PET studies were conducted using the primate mini-EXPLORER long-axial-field-of-view system (1). This system has a 45-cm axial field of view, a 43.5-cm bore diameter, a total National Electrical Manufacturers Association NU-2 sensitivity of 50.2 kcps/MBq, and an isotropic spatial resolution of approximately 3 mm at the center of the field of view. All PET scans were acquired at a single bed position using list-mode data. Immediately after each PET acquisition, a whole-body CT image was acquired on a GE Healthcare Discovery 610 in the same

TABLE 1
Experimental Design

Group	Monkey	Weight (kg)	Age (y)	Injected ^{89}Zr dose (MBq)	Imaging time point after injection (d)
^{89}Zr-DFO-Bz-NCS–anti-gD	A	2.87	1.2	37.4	0, 2, 7, 14, 20, 30
	B	2.87	1.2	36.2	
	C	3.55	1.5	38.8	
^{89}Zr-DFO*-Bz-NCS–anti-gD	A	3.16	1.5	39.5	0, 3, 7, 17, 21, 31
	B	3.35	1.8	36.6	
	C	3.77	2.0	37.4	
^{89}Zr-DFO-squaramide–anti-gD	A	1.75	1.0	42.0	0, 3, 6, 14, 21, 29
	B	1.92	1.0	42.4	
	C	2.24	1.0	43.6	
^{89}Zr-DFO*-squaramide–anti-gD	A	3.00	1.3	47.1	0, 3, 7, 14, 21, 31
	B	2.62	1.2	40.7	
	C	2.25	1.2	41.8	

imaging suite and was coregistered to the PET image. The scan bed was used to carefully move each rhesus monkey between scanners to facilitate accurate image registration without any change in positioning.

Venous blood samples were obtained from each animal at all imaging time points immediately after the CT acquisition. The antibody concentration in the blood samples was quantified via enzyme-linked immunosorbent assay (ELISA).

Image Reconstruction and Quantification

Images were reconstructed using an in-house–developed list-mode time-of-flight ordered-subsets expectation maximization algorithm, including corrections for attenuation, dead time, random coincidences, and radionuclide decay, along with a voxel calibration factor to units of kBq/cm^3. The 511-keV attenuation factors were derived from the coregistered CT image using bilinear scaling (26). No algorithm was used to correct for background signal resulting from the lutetium oxyorthosilicate intrinsic radiation, since the time-of-flight reconstruction sufficiently removes the lutetium oxyorthosilicate coincidence events from the rhesus monkey volume.

Regions of interest were manually extracted from the reconstructed PET images at each time point and used to quantify the mean activity concentration in liver, kidney, blood (mediastinal blood pool), and bone (shoulders and pelvis), as well as the total activity in the body. Activity distributions in each region of interest were quantified using SUV:

$$SUV = \frac{\overline{c_{img}}}{ID/m},$$ Eq. 1

where $\overline{c_{img}}$ is the mean activity concentration in the regions of interest, ID is the total injected dose on day 0, and m is the mass of the animal.

RESULTS

Image Quality

Reconstructed PET images of a single rhesus monkey at all imaging time points are shown in Figure 1. Importantly for this study, the image quality obtained at late time points (days 7–30), even at 30 d after injection, with an absolute residual whole-body activity of less than 40 kBq, was sufficient to identify ^{89}Zr signal in the liver, kidneys, and several sites of uptake at bone epiphyses (shoulder, pelvis, knee). Additionally, excellent image quality was achieved at early time points, clearly capturing the initial antibody distribution throughout the body.

Day 0 Pharmacokinetics

A comparison of early kinetics is demonstrated in Figure 2, showing the dynamic series of images acquired on day 0 from 1 rhesus monkey in each chelator-linker group (subject B; Table 1). As expected for intact antibodies, there was little change in the

^{89}Zr-antibody biodistribution in the first hour after injection because of the slow extraction rate of antibodies from the bloodstream. The behavior observed in the first hour is potentially informative regarding the presence and nature of unwanted low-molecular-weight impurities or degradation products injection.

We noted two important differences in early pharmacokinetics that were likely related to clearance routes. First, both Bz-NCS linker groups showed increasing activity in the bladder toward the end of the 60-min scan, whereas both squaramide linker groups showed very little bladder activity. The bladder activity measured from the last 10-min frame is quantified for all subjects in Figure 3 and showed close agreement with the image assessment. Importantly, high bladder activity for the Bz-NCS linker groups may indicate the presence of low-molecular-weight ^{89}Zr-DFO or ^{89}Zr-DFO* complexes, which are known to be rapidly cleared via the renal system (27,28). The QC purity measurements (Supplemental Figs. 2C and 2D) indicated negligible (<5%) impurities in the squaramide groups out to 3 d after synthesis, as is reflected by the negligible renal clearance in these groups. The Bz-NCS groups (Supplemental Figs. 2A and 2B), on the other hand, exhibited progressively increased low-molecular-weight impurities consistent with unbound ^{89}Zr-DFO-Bz-NCS and ^{89}Zr-DFO*-Bz-NCS and the high bladder activity. However, although the imaging suggested greater impurity levels in the ^{89}Zr-DFO-Bz-NCS material, the QC data showed the opposite: the ^{89}Zr-DFO*-Bz-NCS QC data indicated approximately 3% and 25% impurities at 0 and 5 d after synthesis, respectively, whereas the ^{89}Zr-DFO-Bz-NCS QC data showed approximately 6% and 17% impurities at 0 and 3 d after synthesis, respectively. These results cannot be entirely reconciled, because the imaging and QC samples were separated and handled somewhat differently, with potential for exposure to different conditions of temperature and agitation on the day of transport, for example.

Second, there was an interesting increase in activity in the gastrointestinal tract that was observed in all animals within the DFO-Bz-NCS group but not in any animal within the other 3 chelator-linker groups. Increased gastrointestinal uptake likely represents hepatobiliary clearance of hydrophobic impurities and possibly some fraction of the low-molecular-weight forms of the ^{89}Zr-DFO-linker.

Late-Time-Point Pharmacokinetics

Images acquired at approximately 14 d after injection (DFO*-Bz-NCS group, acquired on day 17) for all rhesus monkeys are shown in Figure 4. Within each chelator-linker group there was little visual variability in the activity biodistributions, whereas easily identifiable differences in activity concentration, such as in the liver, bone, and whole-body, were observed across the 4 groups.

Time–activity curves with SUV$_{mean}$ in the liver, kidneys, bone, blood, and whole body at each imaging time point are shown in Figure 5 for all animals. As suggested from the day 14 image comparisons (Fig. 4), significant differences in uptake in several organs and tissues were measured at late time points across the 4 chelator-linker groups. Within each chelator-linker group, however, there was little variation in the pharmacokinetics for any anatomic site measured.

The main outlying data appear in the day 0 blood activity measurements, where there were large differences in the measured
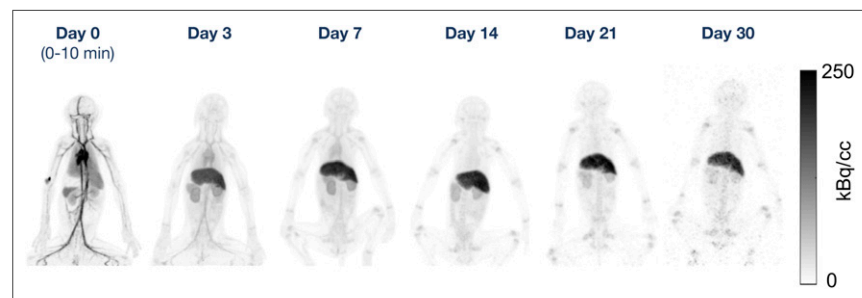

FIGURE 1. Maximum-intensity PET projections at each time point for 1 rhesus monkey in the ^{89}Zr-DFO-squaramide–anti-gD group.
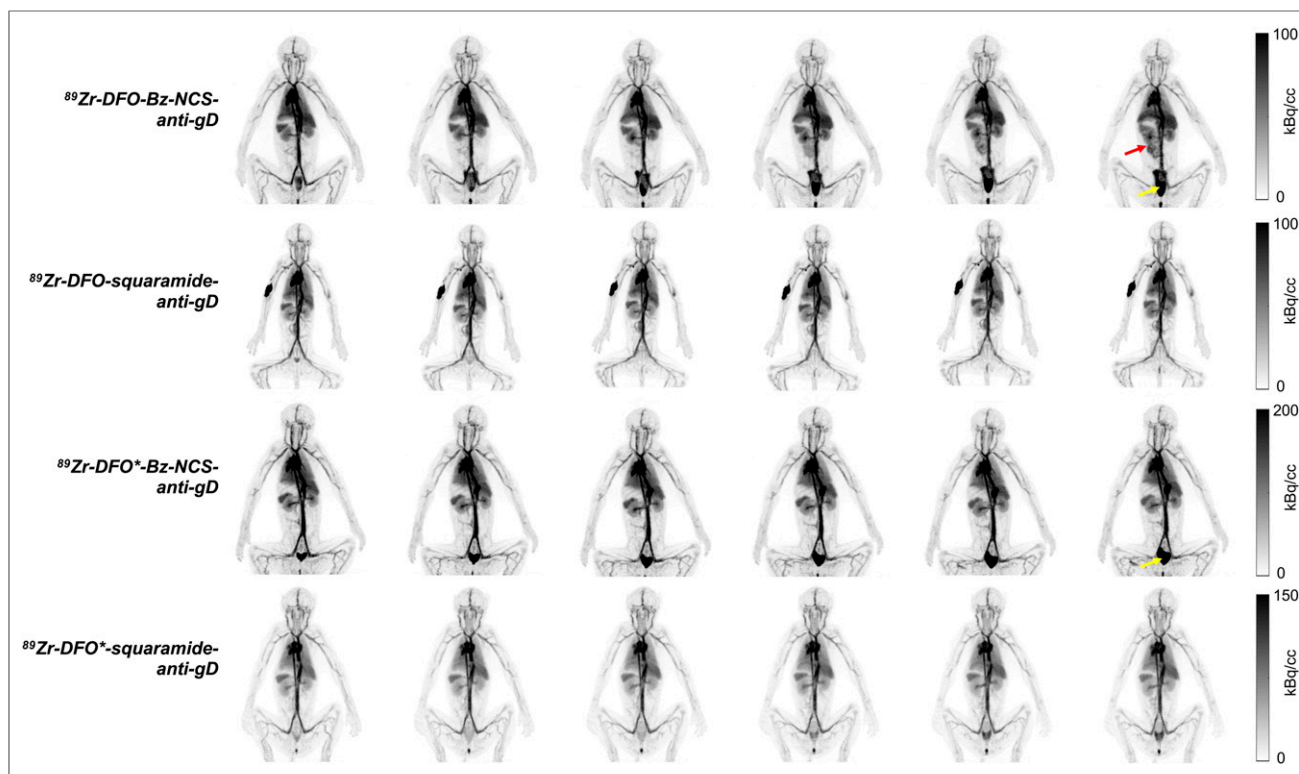
FIGURE 2. Dynamic image sequence acquired on day 0 for rhesus monkey B in each chelator-linker group. Each image is 10-min duration, with first image beginning approximately 2 min after antibody injection. Hot spot in arm of 89Zr-DFO-squaramide–anti-gD group represents activity at injection site. Yellow arrows indicate activity in bladder observed in 89Zr-DFO-Bz-NCS–anti-gD and 89Zr-DFO*-Bz-NCS–anti-gD groups. Red arrow indicates activity in gastrointestinal tract observed only in 89Zr-DFO-Bz-NCS–anti-gD group.

blood activity concentrations across the 3 animals per group within some of the chelator-linker groups (e.g., DFO-Bz-NCS). This contrasts with the consistent whole-body activity values and
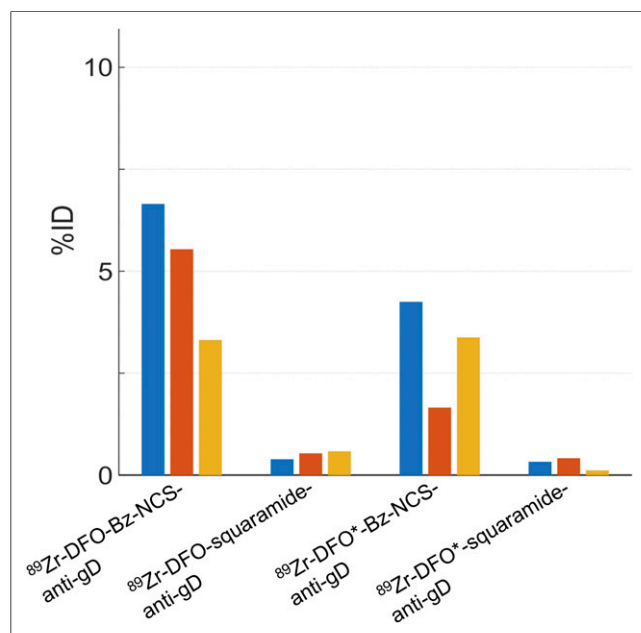

FIGURE 3. Bladder activity measured in last 10-min frame on day 0, approximately 50–60 min after injection. Each bar represents 1 rhesus monkey. %ID = percentage injected dose.

ELISA data. On inspection, it was found that for some of the animals, a fraction of activity remained at the injection site on day 0. This finding might explain some outlier blood activity values on day 0. For example, 2 of the animals in the DFO-Bz-NCS group were found to have approximately 4 and 12.4 MBq of activity, respectively, residing at the injection site at the end of the day 0 scan.

Although there was good agreement between the image-derived blood activity concentration and the ELISA data at later time points, there appeared to be some inconsistencies at the earliest time point, primarily with the DFO-Bz-NCS group. In this group, the image-derived blood activity showed a decline between days 0 and 2 compared with the other 3 chelator-linker groups, whereas the ELISA data were largely consistent across all 4 groups. This inconsistency is presumably related to the presence of low-molecular-weight impurities, as is also suggested by the high bladder clearance on day 0. Additionally, some of the inconsistencies between the image-derived blood activity and the ELISA measurements may be influenced by a fraction of radioactivity (vs. total antibody) at the injection site.

DISCUSSION

In these studies, we demonstrated the feasibility of 30-d duration 89Zr PET imaging studies in rhesus monkeys, enabled through the use of the high-sensitivity primate mini-EXPLORER total-body PET system. Sufficient image quality was maintained throughout the 30-d study (a duration equivalent to approximately 9 radioactive half-lives of 89Zr)—enough to quantify antibody uptake in the liver, kidneys, blood, bone joints, and whole body. Quantitative image
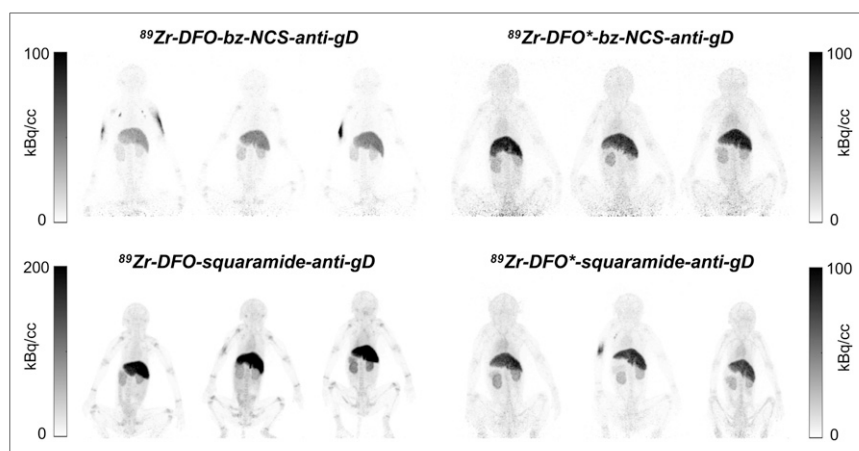
FIGURE 4. Maximum-intensity PET projections acquired on day 14 for all animals. Overall, there is excellent consistency in whole-body activity and uptake in easily identifiable organs and tissues, and differences are noted across groups. Different gray scale is used for ^{89}Zr-DFO-squaramide–anti-gD group. Hot spots in the upper limb of some rhesus monkeys represent residual activity at injection site from day 0. Animal order (left to right) for each group is A, B, and C (Table 1).

outcomes showed that the circulating ^{89}Zr in the plasma mostly remained bound to antibody throughout the experiment, especially once initial low-molecular-weight impurities were discounted, which was an essential step for interpreting DFO-Bz-NCS results (Supplemental Fig. 3).

The study was not designed to suggest optimal formulation conditions for the radiolabeled antibodies used; rather, the formulation used was at the time of the study considered reliable, having been used for commercial therapeutic antibody products and for many small-scale (~MBq labeling) antibody PET studies. We were surprised to find that high levels of low-molecular-weight impurities formed over time and were contained in the injected material in the Bz-NCS linker groups. Consequently, we note the importance of optimizing formulations for shelf-life stab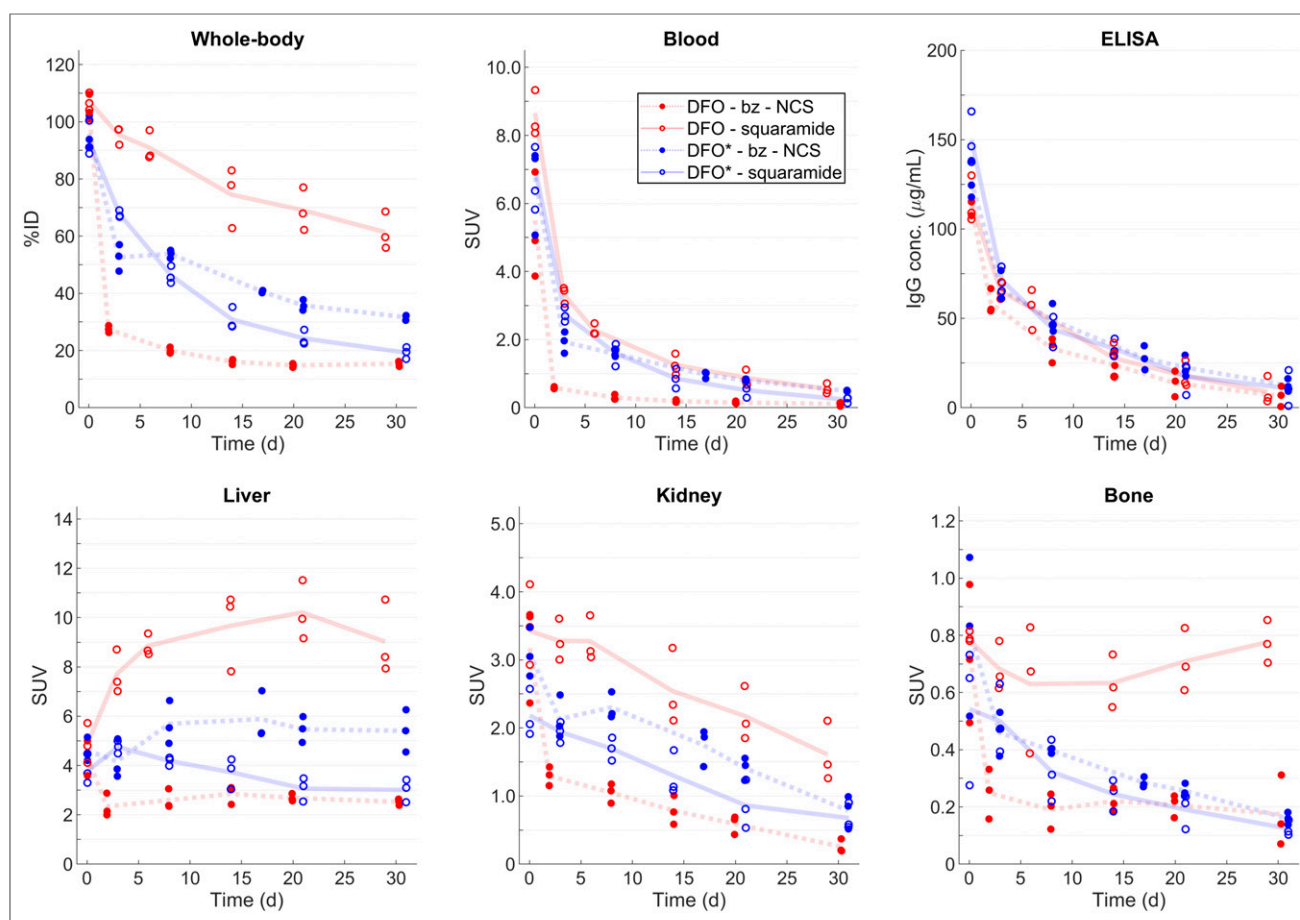ility using labeling, shipping, and QC studies on the same scale as the imaging production runs. Multiday shelf-life stability is a necessary prerequisite to enable distribution of ^{89}Zr tracers and will be important for human clinical studies.

analysis revealed potentially important differences in the 30-d pharmacokinetics associated with 4 different ^{89}Zr chelator-linker combinations and their (implied) catabolites. Comparisons with ELISA

FIGURE 5. Time–activity curves for each region of interest. Markers indicate measurements for each animal, and lines represent mean for each chelator-linker group. Whole-body activity was normalized to injected dose for each subject. %ID = percentage injected dose.

Interestingly, the octadentate DFO*-squaramide and DFO*-Bz-NCS reagents were noted to have markedly less conspicuous uptake at the bone joints than DFO-squaramide ($P < 0.05$ for all time points after day 0). This property may be important to reduce sites of focal uptake that might complicate image interpretation and perhaps pose a risk that nonspecific signal may arise at sites of injury or remodeling associated with metastatic disease.

Conversely, the DFO-squaramide reagent showed substantial conspicuous bone uptake, approximately 3- to 4-fold higher than for all 3 of the other chelator-linker groups at imaging time points later than 7 d after injection, suggesting that this octadentate ligand was not as beneficial to the osteophilic properties of ^{89}Zr catabolites as the DFO*. Even the high bone uptake within the DFO-squaramide group in rhesus monkeys was much lower than the values reported in young mice and rats ($\leq 10\%$–15% of the injected dose at time points later than 3 d after injection) (29).

The DFO-squaramide was also unusual in that, at the end of the 30-d study period, less than 50% of the ^{89}Zr was cleared from the body in all 3 animals per group even though the ELISA showed that the antibody was clearing from the circulation similarly across groups.

Overall, the impurity QC measurements were good predictors of early bladder activity, except for the DFO-Bz-NCS group. This mismatch likely involved greater radiolytic degradation in the sample of ^{89}Zr-labeled antibody transported to the imaging suite without temperature control than in the better-controlled sample retained for the QC testing.

The other major difference between the chelator-linker groups that relates to elimination was observed in the whole-body measurements and was perhaps dominated by the measured liver uptake. Here, the DFO-squaramide group showed substantially higher liver uptake than the other groups ($P < 0.02$ for all time points after day 0). The liver showed uptake because it is a site for antibody catabolism, as well as providing a clearance route for many small molecules, protein and cell aggregates, and colloids such as zirconium-phosphate (29). However, identification of the form of ^{89}Zr-DFO-squaramide persisting in the liver would have required biopsies, which were not performed in this study.

Further investigations could address additional parameters. In particular, we did not include DFO-N-Suc-TFP, perhaps considered the reagent most widely used for clinical antibody PET studies to date. Our priority was to compare DFO and DFO* on the same Bz-NCS linker system and to study the properties of the promising squaramide linker. Future approaches could also address important aspects of the chelator reagents used, such as solubility and behavior in the conjugation process, which might be compared when selecting a chelator-linker combination for antibody PET or similar ^{89}Zr studies. Further work is under way to more fully characterize the various reagents in these terms and to compare in more detail their chemical and imaging properties as they relate to tumor and bone uptake.

Overall, these results suggest that the use of octadentate DFO* gives rise to fewer osteophilic catabolites and a better late time point image signal, presumably the result of a more stable bond complex with ^{89}Zr than is possible with hexadentate DFO. The squaramide linker may also provide some advantages in shelf-life stability when compared with Bz-NCS.

CONCLUSION

The feasibility of extending ^{89}Zr-PET studies for 30 d after injection was demonstrated in these studies using the high-sensitivity primate mini-EXPLORER PET system. Using a cohort of 12 young rhesus monkeys, we evaluated the pharmacokinetics associated with 4 ^{89}Zr chelator-linkers in combination with humanized IgG antibodies. Quantitative image analysis suggested that using the octadentate chelator DFO* results in improved ^{89}Zr chelating stability, as evidenced by differences in bone and liver uptake at the later time points. Overall, excellent consistency was observed within each group even at very late time points and enabled the observation of interesting differences in tissue and bone uptake with the various chelators and linkers. The results also suggest that careful selection of reagents and rigorous assessment of shelf-life stability are warranted for future studies.

KEY POINTS

QUESTION: Is quantitative ^{89}Zr-antibody PET imaging feasible up to 30 d after injection, and if so, what is the in vivo behavior of several common DFO-variant chelators over this duration?

PERTINENT FINDINGS: Accurate quantification indicated by highly consistent pharmacokinetics within each chelator-linker group was maintained over the 30-d study duration because of the high sensitivity of the long-axial-field-of-view PET system. Significant differences were observed in the pharmacokinetics associated with each chelator-linker moiety, attributed to differences in both in vivo behavior and shelf-life stability.

IMPLICATIONS FOR PATIENT CARE: The feasibility of long-duration ^{89}Zr imaging with total-body PET enables physiologically optimized imaging time points that are not limited by scanner sensitivity. The chelator pharmacokinetics comparison is a necessary prerequisite to enable distributed use of ^{89}Zr tracers for human clinical studies.

REFERENCES

1. Berg E, Zhang X, Bec J, et al. Development and evaluation of mini-EXPLORER: a long axial field-of-view PET scanner for non-human primate imaging. *J Nucl Med.* 2018;59:993–998.
2. Lv Y, Lv X, Liu W, et al. Mini EXPLORER II: a prototype high-sensitivity PET/CT scanner for companion animal whole body and human brain scanning. *Phys Med Biol.* 2019;64:075004.
3. Badawi RD, Shi H, Hu P, et al. First human imaging studies with the EXPLORER total-body PET scanner. *J Nucl Med.* 2019;60:299–303.
4. Karp J, Schmall J, Geagan M, et al. Imaging performance of the PennPET Explorer scanner [abstract]. *J Nucl Med.* 2018;59(suppl 1):222.
5. Cherry SR, Jones T, Karp JS, et al. Total-body PET: maximizing sensitivity to create new opportunities for clinical research and patient care. *J Nucl Med.* 2018;59:3–12.
6. van Dongen GA, Visser GW, Lub-de Hooge MN, et al. Immuno-PET: a navigator in monoclonal antibody development and applications. *Oncologist.* 2007;12:1379–1389.

7. van Dongen GA, Vosjan MJ. Immuno-positron emission tomography: shedding light on clinical antibody therapy. *Cancer Biother Radiopharm.* 2010;25:375–385.

8. Vugts DJ, Visser GW, van Dongen GA. [89]Zr-PET radiochemistry in the development and application of therapeutic monoclonal antibodies and other biologicals. *Curr Top Med Chem.* 2013;13:446–457.

9. Tarantal AF, Lee CCI, Kukis DL, et al. Radiolabeling human peripheral blood stem cells for positron emission tomography (PET) imaging in young rhesus monkeys. *PLoS One.* 2013;8:e77148.

10. Sato N, Wu H, Asiedu KO, et al. [89]Zr-oxine complex PET cell imaging in monitoring cell-based therapies. *Radiology.* 2015;275:490–500.

11. Keliher EJ, Yoo J, Nahrendorf M, et al. [89]Zr-labeled dextran nanoparticles allow in vivo macrophage imaging. *Bioconjug Chem.* 2011;22:2383–2389.

12. Ruggiero A, Villa CH, Holland JP, et al. Imaging and treating tumor vasculature with targeted radiolabeled carbon nanotubes. *Int J Nanomedicine.* 2010;5:783–802.

13. Deri MA, Zeglis BM, Francesconi LC, et al. PET imaging with [89]Zr: from radiochemistry to the clinic. *Nucl Med Biol.* 2013;40:3–14.

14. Fischer G, Seibold U, Schirrmacher R, et al. [89]Zr, a radiometal nuclide with high potential for molecular imaging with PET: chemistry, applications and remaining challenges. *Molecules.* 2013;18:6469–6490.

15. Bansal A, Pandey MK, Demirhan YE, et al. Novel [89]Zr cell labeling approach for PET-based cell trafficking studies. *EJNMMI Res.* 2015;5:19.

16. Ulaner GA, Hyman DM, Ross DS, et al. Detection of HER2-positive metastases in patients with HER2-negative primary breast cancer using [89]Zr-trastuzumab PET/CT. *J Nucl Med.* 2016;57:1523–1528.

17. Bhatt NB, Pandya D, Wadas T. Recent advances in zirconium-89 chelator development. *Molecules.* 2018;23:E638.

18. Perk LR, Vosjan MJ, Visser GW, et al. p-isothiocyanatobenzyl-desferrioxamine: a new bifunctional chelate for facile radiolabeling of monoclonal antibodies with zirconium-89 for immuno-PET imaging. *Eur J Nucl Med Mol Imaging.* 2010;37:250–259.

19. Verel I, Visser GW, Boellaard R, et al. [89]Zr immuno-PET: comprehensive procedures for the production of [89]Zr-labeled monoclonal antibodies. *J Nucl Med.* 2003;44:1271–1281.

20. Dijkers EC, Munnink TO, Kosterink J, et al. Biodistribution of [89]Zr-trastuzumab and PET imaging of HER2-positive lesions in patients with metastatic breast cancer. *Clin Pharmacol Ther.* 2010;87:586–592.

21. Holland JP, Evans MJ, Rice SL, et al. Annotating MYC status with [89]Zr-transferrin imaging. *Nat Med.* 2012;18:1586–1591.

22. Vugts DJ, Klaver C, Sewing C, et al. Comparison of the octadentate bifunctional chelator DFO*-pPhe-NCS and the clinically used hexadentate bifunctional chelator DFO-pPhe-NCS for [89]Zr-immuno-PET. *Eur J Nucl Med Mol Imaging.* 2017; 44:286–295.

23. Patra M, Bauman A, Mari C, et al. An octadentate bifunctional chelating agent for the development of stable zirconium-89 based molecular imaging probes. *Chem Commun (Camb).* 2014;50:11523–11525.

24. Rudd SE, Roselt P, Cullinane C, et al. A desferrioxamine B squaramide ester for the incorporation of zirconium-89 into antibodies. *Chem Commun (Camb).* 2016; 52:11889–11892.

25. Vosjan MJ, Perk LR, Visser GW, et al. Conjugation and radiolabeling of monoclonal antibodies with zirconium-89 for PET imaging using the bifunctional chelate p-isothiocyanatobenzyl-desferrioxamine. *Nat Protoc.* 2010;5:739–743.

26. Carney JP, Townsend DW, Rappoport V, et al. Method for transforming CT images for attenuation correction in PET/CT imaging. *Med Phys.* 2006;33: 976–983.

27. Abou DS, Ku T, Smith-Jones PM. In vivo biodistribution and accumulation of [89]Zr in mice. *Nucl Med Biol.* 2011;38:675–681.

28. Meijs WE, Haisma HJ, Van Der Schors R, et al. A facile method for the labeling of proteins with zirconium isotopes. *Nucl Med Biol.* 1996;23:439–448.

29. Holland JP, Divilov V, Bander NH, et al. [89]Zr-DFO-J591 for immunoPET imaging of prostate-specific membrane antigen (PSMA) expression in vivo. *J Nucl Med.* 2010;51:1293–1300.